

# Transfer function approaches for SEEG brain electrode interface applied to tissue classification

Mariana Mulinari Pinheiro Machado  
 Univ. Grenoble Alpes, CNRS, Grenoble INP  
 GIPSA-lab  
 Grenoble, France  
<https://orcid.org/0000-0002-1635-4714>

Alina Voda  
 Univ. Grenoble Alpes, CNRS, Grenoble INP  
 GIPSA-lab  
 Grenoble, France  
<https://orcid.org/0000-0001-8138-5499>

Gildas Besançon  
 Univ. Grenoble Alpes, CNRS, Grenoble INP  
 GIPSA-lab  
 Grenoble, France  
<https://orcid.org/0000-0001-5701-6255>

Guillaume Becq  
 Univ. Grenoble Alpes, CNRS, Grenoble INP  
 GIPSA-lab  
 Grenoble, France  
<https://orcid.org/0000-0002-2134-1803>

Philippe Kahane  
 Univ. Grenoble Alpes, CHU Grenoble Alpes  
 Grenoble Institut des Neurosciences, GIN  
 Grenoble, France  
<https://orcid.org/0000-0003-1330-3281>

Olivier David  
 Aix Marseille Univ., Inserm, INS  
 Institut de Neurosciences des Systèmes  
 Marseille, France  
<https://orcid.org/0000-0003-0776-0216>

**Abstract**—This paper is about transfer function approaches for brain-electrode interface modelling in the context of StereoElectroEncephaloGraphy, and their possible use in tissue classification (between grey and white matter). Monopolar and bipolar configurations are first reviewed, giving rise to possible non-parametric and parametric identification methods, as well as related possible classification results (for identical tissues and distinct tissues at measurement points, respectively). A method combining both approaches is then proposed, so as to end up with a classification at each measurement point in any case. The proposed methodology is implemented with clinical data collected from a set of epileptic patients, confirming its interest by providing more than 70% of accuracy in the obtained results.

**Index Terms**—SEEG, dynamical modelling, system identification, classification, clinical data.

## I. INTRODUCTION

Epilepsy is characterized by interruption of normal brain functioning [10], and in front of focal drug-resistant cases, resective surgery of the so-called *epileptogenic zone* (EZ) may become necessary [3]. This requires appropriate identification of the EZ, which can be done by non-invasive methods, or by invasive ones for more difficult cases. StereoElectroEncephaloGraphy (SEEG), where electrodes are inserted into the patient's brain, enters in the latter situation (as illustrated by Figure 1).

In that case, distinguishing between grey and white matters for the tissue where each electrode contact is located becomes an important preliminary task: firstly because white matter

This research has been supported in part by IDEX 2018 FracPhab project, Grenoble INP, France, by Grenoble-Alpes University Hospital (EPISTIM Project no. 1325, ID RCB 2013-A01098-37), by International Collaborative Research Project ANR-DFG (RFTC project, ANR-18-CE92-0053-01) and by the European Research Council via the European Union's Seventh Framework Programme (FP/2007-2013)/ERC Grant Agreement no. 616268 F-TRACT, together with the European Union's Horizon 2020 Framework Programme for Research and Innovation via Specific Grant Agreement No. 785907 and 945539 (Human Brain Project SGA2 and SGA3).

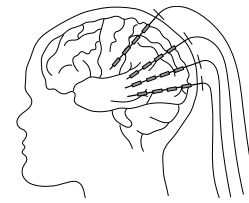


Fig. 1: SEEG

not being epileptogenic [11], related contacts should be disregarded; secondly because in functional connectivity analysis, stimulations in grey and white matters should not be the same [31], as they produce different effects [25].

Classically, distinguishing between grey and white matter is based on co-registration of structural Magnetic Resonance Imaging (MRI) with Computed Tomography (CT) scans [9], which can be limited by poor image quality, e.g. geometrical distortion and poor contrast between grey and white matter. This motivates for searching alternatives, directly using SEEG signals. Very few studies have investigated such an approach: a Bayesian classifier has been recently considered in [11], based on features extracted from signals in a bipolar montage, while we have started to explore system identification methods in [18] and [21].

In [18], features were proposed on the basis of non-parametric identification of frequency response between pairs of consecutive contacts, providing a promising accuracy for pairs in homogeneous matter, as compared to MRI classification. In [21], a parametric model of the brain-electrode interface was proposed based on triplets of consecutive contacts, giving again classification results with a good accuracy, but for triplets in heterogeneous matter.

Those results were obtained by considering previously selected homogeneous pairs and heterogeneous triplets of con-

tacts respectively. This means that none of the methods were used for tissue classification at a given contact without any prior knowledge about tissue homogeneity or heterogeneity w.r.t. its neighbours.

In this context, *the main goal of the present paper is to show how transfer function approaches and related system identification can be used for automatic brain tissue classification at every single contact, directly using SEEG signals.*

This combines our former communications [19], [20] enhancing both the modelling approach and the classification one.

About modelling, we refer to that of the brain-electrode interface which is involved. This topic has been considered in various studies, more particularly in the context of Deep Brain Stimulation (DBS), to quantify impedance changes. In [26], [15], [14], or [30] for instance, a model has been identified via electrode impedance spectroscopy (EIS) or impedance tester, using signals recorded in animals chronically implanted with electrodes. In such experiments, the impedance between electrode contacts is identified by measuring both contact voltages and the current in between. In the context of SEEG, one can only find [4] where an impedance model was identified, but again using a known current - and with a simpler structure. However, in usual SEEG conditions, the current is not measured, and the only available information reduces to voltage measurements at each contact.

An additional difficulty in such available studies is that most models include derivation operators of *non-integer order*, in so-called *Constant Phase Elements (CPE)*. Non-integer order (or fractional order) derivatives, which extend standard derivation [28], have been introduced in the modelling of various physical systems for their improved memory properties [27]. They can also be found in biological systems (as in [22], [13], [32] for instance), and were in particular successfully used in our previous study of a phantom EEG measurement device [1]. As in [21], we will here consider a non-integer order model. Regarding classification, the main idea in this paper is to combine approaches formerly developed for homogeneous and heterogeneous cases in [18] and [21] respectively, so as to obtain single contact classification.

The remainder of the paper is organized as follows: section II first provides an overview on the modelling methodology, and section III continues with corresponding identification approaches, together with related classification results. On this basis, section IV then proposes a single contact classification scheme, and section V finally concludes the paper.

## II. TRANSFER FUNCTION MODELLING FOR BRAIN TISSUE CLASSIFICATION

### A. Transfer function approach

Transfer function approach means defining input and output variables. In the context of SEEG, the known information is related to contact voltages, which can thus be used for such definitions. The dynamics in between corresponds to the brain-electrode interface behaviour, which, as mentioned

before, has been largely studied in the literature. In particular it can be characterized by three elements, as depicted by Figure 2: a so-called *peri-electrode* layer (corresponding to tissue encapsulation of the electrode formed by the brain reaction to foreign bodies), a direct *interface* between each contact and its surrounding physiological tissue, and the *brain* tissue itself.

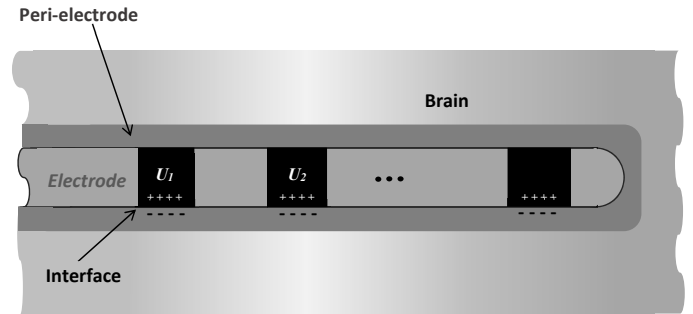


Fig. 2: Physical representation of the brain-electrode interface (with electrode contacts in black).

Each of these elements can be described by its impedance, as emphasized by Figure 3:  $Z_i$  for interface impedance,  $Z_p$  for peri-electrode one, and  $Z_b$  for brain one, for which previous studies provide electrical models.

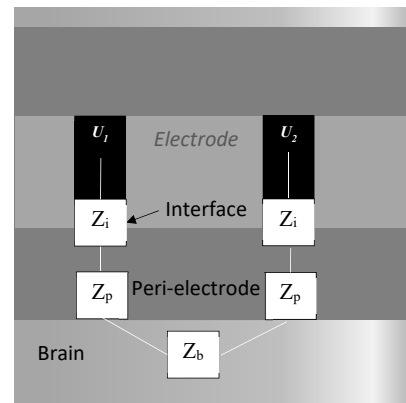


Fig. 3: Impedance representation between contacts.

Notice that in this representation, interface and peri-electrode impedances are identical for the two contacts. In fact, no difference in interface or peri-electrode impedances according to the nature of the surrounding brain tissue (grey or white matter) has been reported in the literature. Hence we can make the simplifying assumption that they are uniform all along the electrode. On the other hand, it has been observed that grey and white matters have different conductivities [4], [24]. Therefore, these differences should have an impact on the transfer function, which can in turn be used for tissue classification.

The overall impedance between two consecutive contacts (say  $U_1, U_2$ ) is summarized by Figure 4, and two approaches can then be considered, either non-parametric, or parametric

(following the terminology of [17] for instance).

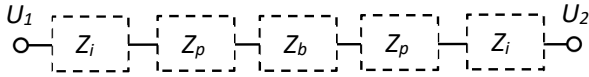


Fig. 4: Electrical impedance between two contacts.

### B. Non-parametric approach

In a first approach, the transfer between measured contact voltages can be considered in a standard monopolar configuration, where each voltage is taken w.r.t. a common reference contact ( $U_{ref}$ ) located away in white matter: for instance  $V_{1ref} = U_1 - U_{ref}$ ,  $V_{2ref} = U_2 - U_{ref}$ , for two consecutive contacts  $U_1, U_2$ . This amounts to a transfer function as in Figure 5 (with  $V_{1ref}$  as the input,  $V_{2ref}$  as the output, and appropriate impedances  $Z_{12}, Z_{1ref}$ ).

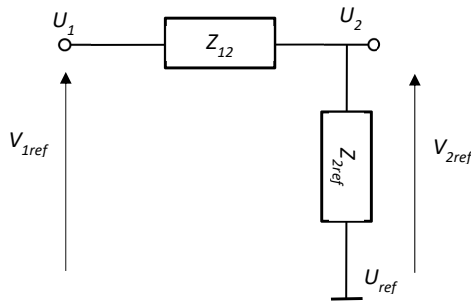


Fig. 5: Monopolar montage: voltage measurements at two consecutive contacts  $U_1$  and  $U_2$  are taken w.r.t. a distant contact  $U_{ref}$ .

Following our former study [18], such a configuration can give rise to direct frequency response identification between measurements for pairs of consecutive SEEG contacts. Examples of identified models in such a way are given in Figure 6, where mean magnitudes of Bode plots obtained for 19 patients at rest, and a total of 486 pairs of contacts [18], are displayed. It can be noticed that the magnitude profile looks like that of a so-called lag-lead filter.

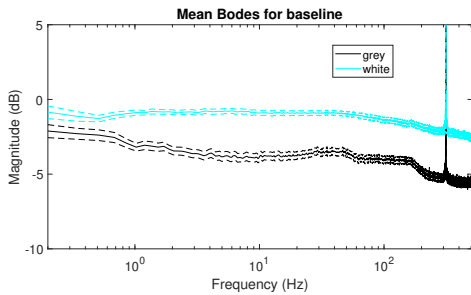


Fig. 6: Mean frequency response of pairs of contacts in grey matter (in black), and white matter (in cyan) (from [18]).

### C. Parametric approach

In order to enhance the transfer function approach, a parametric model can also be considered [21]: the idea is then to rely on available electrical descriptions of  $Z_i, Z_p, Z_b$ . Here it can be noticed that the impedance w.r.t.  $U_{ref}$  ( $Z_{2ref}$  in Figure 5) is not easily deduced, in particular because it may vary according to the position of the considered contact. For this reason, we now adopt a bipolar configuration, where each voltage in a pair of consecutive contacts ( $U_1, U_2$ ) is referenced w.r.t. the next adjacent one (denoted by  $U_0$ ):

$$\begin{aligned} V_1 &:= U_1 - U_0 = V_{1ref} - V_{0ref} \\ V_2 &:= U_2 - U_0 = V_{2ref} - V_{0ref} \end{aligned} \quad (1)$$

with  $V_{0ref} := U_0 - U_{ref}$ . This approach is summarized by Figure 7 (where  $Z$  gathers  $Z_i$  and  $Z_p$ , and index  $i = 1, 2$  for  $Z_b$  refers to possible variations in brain impedance).

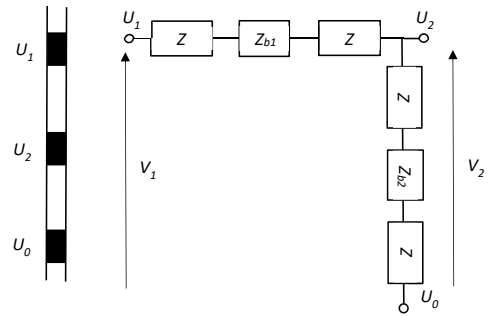


Fig. 7: Bipolar montage: voltage measurements at two consecutive contacts  $U_1$  and  $U_2$  are taken w.r.t. subsequent contact  $U_0$ .

Representations of impedances  $Z_i, Z_p, Z_b$  are recalled next:

1) *Interface*: One of the first contributions towards an electrical representation for it can be found in [29]: the proposed model is made of a double layer capacitance  $C_{dl}$ , representing the charge layers in the metal surface and the peri-electrode one (as shown in Figure 2), in parallel with a charge transfer resistance  $R_{ct}$ , corresponding to charge leaks due electrochemical reactions. It was then shown that to better account for adsorption, surface roughness, and molecular forces in the capacitive effect [6], capacitance  $C_{dl}$  can be replaced by a capacitance with non-integer order model (Constant Phase Element), of the following form:

$$Z_{CPE_{dl}}(s) = \frac{1}{Q_{dl} s^\alpha} \quad (2)$$

for a constant  $Q_{dl}$ , and  $s$  the Laplace variable.

Here  $0 < \alpha < 1$ , represents the non-integer order, and the inverse Laplace transform of  $s^\alpha$  corresponds to a fractional-order time derivative (see e.g. [16]).

The corresponding interface impedance model  $Z_i$  is illustrated by Figure 8.

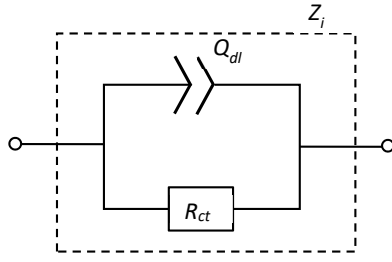


Fig. 8: Interface impedance model.

2) *Peri-electrode*: The *peri-electrode* characterizes the encapsulation layer that appears around the implanted electrode by reaction of nervous system [12]. In SEEG measurements, electrodes are implanted long enough so that such a phenomenon occurs [15]. An electrical circuit to represent it can be found for instance in [26], [15], and [30]: it takes the form of a resistor, representing the encapsulation tissue by extracellular matrix proteins ( $R_{en}$ ), in series with an RC parallel circuit, capturing the physical properties of the glial cell membrane that surrounds the electrode. The model can again be improved by replacing the standard capacitor with a CPE ( $Z_{CPE_{cl}}$ , as in equation (2), with a constant  $Q_{cl}$ ) [15], still in parallel with a resistor ( $R_{cl}$ ). The resulting model for the *peri-electrode* impedance is given in Figure 9.

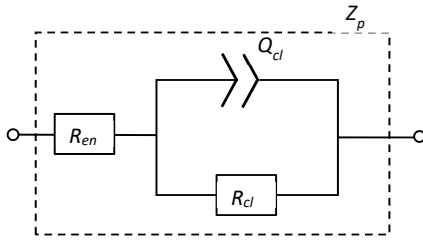


Fig. 9: Peri-Electrode impedance model.

3) *Brain*: The third element involved is the brain itself, which can be represented by a simple resistor  $R_{med}$  characterizing the resistance of the propagation medium between the measuring contacts. Its illustration  $Z_b$  reduces to that of Figure 10.

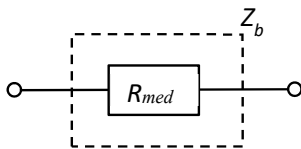


Fig. 10: Brain impedance model.

Notice that in addition to considering that  $Z_i$  and  $Z_b$  are the same ones at each contact, we will assume that non-integer orders in both CPE's involved in this model are identical, consistently with results of [15] for instance.

Finally, the transfer function between  $V_1$  and  $V_2$  is given by the following:

*Proposition 1*: Considering electrical circuit of Figure 7, with elements of Figures 8, 9, 10, the transfer function  $\mathcal{L}(V_2)(s)/\mathcal{L}(V_1)(s)$  reads

$$G_{12}(s) = \frac{\mathcal{L}(V_2)(s)}{\mathcal{L}(V_1)(s)} = \frac{B_1 s^{2\alpha} + B_2 s^\alpha + B_3}{A_1 s^{2\alpha} + A_2 s^\alpha + 1} \quad (3)$$

where  $\mathcal{L}(\cdot)$  stands for the Laplace transform, and coefficients  $B_i$ 's,  $A_i$ 's are given by:

$$B_1 = \frac{Q_{dl} Q_{cl} R_{ct} R_{cl} (R_{med2} + 2R_{en})}{4R_{ct} + 4R_{cl} + 4R_{en} + R_{med1} + R_{med2}} \quad (4)$$

$$B_2 = \frac{(Q_{dl} R_{ct} + Q_{cl} R_{cl})(2R_{en} + R_{med2})}{4R_{ct} + 4R_{cl} + 4R_{en} + R_{med1} + R_{med2}} + \frac{2R_{ct} R_{cl} (Q_{cl} + Q_{dl})}{4R_{ct} + 4R_{cl} + 4R_{en} + R_{med1} + R_{med2}} \quad (5)$$

$$B_3 = \frac{2R_{ct} + 2R_{cl} + 2R_{en} + R_{med2}}{4R_{ct} + 4R_{cl} + 4R_{en} + R_{med1} + R_{med2}} \quad (6)$$

$$A_1 = \frac{Q_{dl} Q_{cl} R_{ct} R_{cl} (4R_{en} + R_{med1} + R_{med2})}{4R_{ct} + 4R_{cl} + 4R_{en} + R_{med1} + R_{med2}} \quad (7)$$

$$A_2 = \frac{4R_{ct} R_{cl} (Q_{dl} + Q_{cl})}{4R_{ct} + 4R_{cl} + 4R_{en} + R_{med1} + R_{med2}} + \frac{(4R_{en} + R_{med1} + R_{med2})(R_{ct} Q_{dl} + R_{cl} Q_{cl})}{4R_{ct} + 4R_{cl} + 4R_{en} + R_{med1} + R_{med2}} \quad (8)$$

□

This can be established by simple impedance composition and voltage divider law (see appendix for more details).

It can be noticed from equation (3) that in low frequencies the gain becomes  $G_{12}(s \rightarrow 0) \rightarrow B_3$ , while in high frequencies we have  $G_{12}(s \rightarrow \infty) \rightarrow B_1/A_1$ . Thus, this model can represent either a lag-lead or a lead-lag behaviour, depending on the values of  $B_1$ ,  $B_3$ , and  $A_1$ , with a plateau in low frequencies and another one in high frequencies. This is illustrated by Figure 6 hereafter, where the magnitude of frequency response is displayed for five versions of transfer function (3), computed for different values of electrical components. In those models, the non-integer order has been set to 0.8, as a typical value in such biomedical systems [23], [2], and each electrical parameter has been chosen randomly in the following sets, consistently with results already presented in the literature [29], [15], [21]:  $1k\Omega < R_r < 1M\Omega$ ,  $100pF < C_s < 100nF$ ,  $10nF < Q_{dl} < 15\mu F$ ,  $10nF < Q_{cl} < 15\mu F$ ,  $1k\Omega < R_{ct} < 200k\Omega$ ,  $1k\Omega < R_{cl} < 50k\Omega$ ,  $1k\Omega < R_{en} < 10k\Omega$ , and  $1k\Omega < R_{med} < 30k\Omega$ .

Notice that a parametric model for the monopolar montage can also be considered, but it appears to be less suitable to represent the expected lag-lead behavior [19], and is thus omitted here.

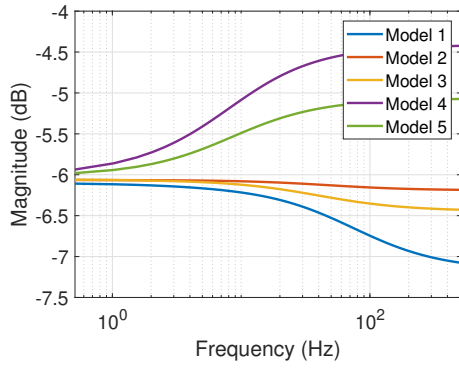


Fig. 11: Examples of magnitude profiles in bode plots of five different simulated models using the proposed circuit with five different sets of electrical parameters.

### III. IDENTIFICATION TOOLS AND BACKGROUND MULTI-CONTACT RESULTS

#### A. Data and identification methodology

Let us consider here similar data as in our former works [18], [21]: they come from actual SEEG recordings on 19 drug-resistant adult epileptic patients at the Hospital of Grenoble-Alpes University, who consented to the re-use of their data by research protocol F-TRACT (INSERM IRB 14-140). Signals have been collected via a Micromed (Treviso, Italy) SEEG/video system in monopolar montage, with sampling frequency  $f_s = 512 \text{ Hz}$  for 12 patients, and  $1024 \text{ Hz}$  for the other 9. A band-pass filter with frequency range between  $0.1$  and  $200 \text{ Hz}$  was used, and all data resampled at  $256 \text{ Hz}$  (see chapter 14 of [17]). Electrodes come from Dixi Medical (Besançon, France), and were implanted by 6 to 15 per patient. Each of them contains 5 to 18 contacts, with a length equal to  $1.5 \text{ mm}$ , a diameter of  $0.8 \text{ mm}$ , and contact inter-distance equal to  $3.5 \text{ mm}$  (from center to center).

The tissue in which each contact is inserted in was classified using MRI co-registration with CT-scan, following the procedure of [7] and using FreeSurfer software. This classification is used as the gold reference in this whole study.

Notice that for all our classifications, we use Linear Discriminant Analysis (LDA).

Notice also that as in [18], [21], we only consider baseline signals here, over  $40 \text{ s}$  in time, and recorded at rest [5].

On the basis of such data, and following the discussion of section II, two different transfer function models can be considered, giving rise to two different identification approaches: either frequency response identification, based on pairs of contacts, or impedance-based (non-integer order) parametric model, based on triplets of contacts. It appears that the first approach allows to distinguish between grey and white matters when the tissue looks homogeneous between the two contacts of a considered pair (either Grey/Grey or White/White). On the other hand, the second approach is appropriate for tissue classification in case of heterogeneity

(Grey/White or White/Grey). The corresponding identification tools and results are reviewed hereafter.

#### B. Pairs of contacts with homogeneous tissues

In this approach, monopolar montage of Figure 5 is considered, with outermost contact taken as the input ( $V_{1ref}$ ), and innermost contact as the output ( $V_{2ref}$ ) for each contact pair, as in Figure 12.

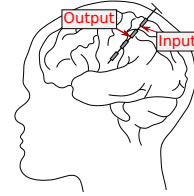


Fig. 12: Input and output contact ordering.

The frequency response is estimated via Spectral Analysis (SPA) (see chapter 6 of [17]) as follows:

$$\hat{G}_{SPA}(e^{i\omega}) = \frac{\hat{\Phi}_{V_{2ref}V_{1ref}}(\omega)}{\hat{\Phi}_{V_{1ref}}(\omega)} \quad (9)$$

where  $\hat{\Phi}_{V_{2ref}V_{1ref}}(\omega)$  is the Fourier transform of the windowed cross-covariance between input and output signals, and  $\hat{\Phi}_{V_{1ref}}(\omega)$ , the Fourier transform of the windowed covariance of input signal  $V_{1ref}$ , both being functions of pulsation  $\omega$  (or of frequency  $f$ , via  $\omega = 2\pi f$ ).

In polar form, this expression gives magnitude  $\hat{M}_{SPA}(\omega)$ , and phase  $\hat{\phi}_{SPA}(\omega)$  of the frequency response, as:

$$\hat{G}_{SPA}(e^{i\omega}) = \hat{M}_{SPA}(\omega)e^{i\hat{\phi}_{SPA}(\omega)} \quad (10)$$

From the frequency response analysis of [18], four discriminant features can be considered, defined from magnitude  $\hat{M}_{SPA}(\omega)$ , as mean squares ( $MS$ ) and relative mean squares ( $RMS$ ), over two frequency ranges:  $FR_1 = [0 \text{ Hz}, 30 \text{ Hz}]$  and  $FR_2 = [30 \text{ Hz}, 128 \text{ Hz}] = [30 \text{ Hz}, f_s/2 \text{ Hz}]$ :

$$MS_{FRi} = \frac{1}{N_i} \sum_{f_j \in FR_i} \hat{M}_{SPA}^2(2\pi f_j) \quad (11)$$

$$RMS_{FRi} = \frac{MS_{FRi}}{MS_b} \quad (12)$$

with  $i = \{1, 2\}$ ,  $N_i$  the number of samples within frequency range  $FR_i$ , and  $MS$  the mean square over the full frequency range  $FR_1 \cup FR_2$ .

Focusing on homogeneous pairs of contacts (either both in grey matter, or both in white matter) according to MRI classification in our data set, and after elimination of outliers, 1058 pairs are left. Considering fifty scenarios of different training data (90% of the data) and test data (10%), an accuracy of  $72 \pm 3\%$  could finally be obtained in the classification results.

### C. Triplets of contacts with heterogeneous tissues

In this approach, the idea is to exploit the physical interpretation of the parametric model given in proposition 1, to obtain other features for classification [21].

Taking indeed advantage of the resistance variation w.r.t. the brain matter nature (grey or white), the primary idea is to use the estimation of  $R_{med}$  parameter as a feature, for each available triplet of contact.

Noting that model (3) is characterized by a vector of 5 parameters  $\theta = [B_1, B_2, B_3, A_1, A_2]^T$ , while they depend on 7 electrical parameters, it is not possible to recover all electrical ones from estimates of  $\theta$ .

However, it appears from equations (7) and (4) that for a given triplet of contacts,  $R_{med1}$  and  $R_{med2}$  can be compared as follows:

*Proposition 2:* From relations (7) and (4) we have:

$$\frac{B_1}{A_1} > 0.5 \Leftrightarrow R_{med2} > R_{med1} \quad (13)$$

$$\frac{B_1}{A_1} = 0.5 \Leftrightarrow R_{med2} = R_{med1} \quad (14)$$

□

The proof is obvious (just noting that we have  $\frac{B_1}{A_1} = \frac{2R_{en} + R_{med2}}{4R_{en} + R_{med1} + R_{med2}}$ ).

From this result, when the brain matter is different between all contacts in a triplet ( $R_{med2} \neq R_{med1}$ ), then  $\frac{B_1}{A_1}$  becomes a possible feature to distinguish between them.

Estimates for  $B_1$  and  $A_1$  can be obtained by parametric identification of model (3). Re-written in time-domain, it reads:

$$A_1 \left( \frac{d}{dt} \right)^{2\alpha} V_2(t) + A_2 \left( \frac{d}{dt} \right)^{\alpha} V_2(t) + V_2(t) = B_1 \left( \frac{d}{dt} \right)^{2\alpha} V_1(t) + B_2 \left( \frac{d}{dt} \right)^{\alpha} V_1(t) + B_3 V_1(t) \quad (15)$$

Following former discussions of [8], [33], [2] on non-integer order identification via regression, the non-integer order time derivative of a signal  $V$  can be approximated from its discrete values  $V(k)$  at times  $kh$  (with sampling time  $h$ ) for  $N$  samples, by Grünwald–Letnikov method, as follows [28]:

$$\left( \frac{d}{dt} \right)^{\alpha} V(k) \simeq \frac{1}{h^{\alpha}} \sum_{i=0}^N (-1)^i \binom{\alpha}{i} V(k-i) \quad (16)$$

with  $\binom{\alpha}{i}$  the generalised Newton binomial.

Equation (15) is then turned into a linear regression [21]:

$$V_2(k, \theta_d) = \varphi^T(k) \theta_d \quad (17)$$

where  $V_2(k, \theta_d)$  represents our model output.

In this regression, the parameter vector is:

$$\theta_d = \theta \frac{h^{2\alpha}}{h^{2\alpha} + \theta_4 + \theta_5 h^{\alpha}} \quad (18)$$

where  $\theta_i$  is the  $i$ th component of  $\theta$ , and the regressor is:

$$\varphi(k) = [F_{2\alpha}(V_1)(k), F_{\alpha}(V_1)(k), V_1(k), F_{2\alpha}(V_2)(k-1), F_{\alpha}(V_2)(k-1)]^T \quad (19)$$

where  $F_{\gamma}(\cdot)$  refers to a filter operator, related to some non-integer order  $\gamma$ , and defined from delay operator  $q$  by:

$$F_{\gamma} = \frac{1}{h^{\gamma}} \sum_{i=0}^N (-1)^i \binom{\gamma}{i} q^{-i} \quad (20)$$

The identification finally becomes a minimisation problem:

$$\min_{\theta_d} \frac{1}{N} \sum_k (V_2(k) - V_2(k, \theta_d))^2 \quad (21)$$

where  $V_2(k)$  is the actual measurement of  $V_2$  at time  $kh$ .

In this formulation, additional constraints can be added, so as to respect positivity of parameters typically.

From estimate  $\hat{\theta}_d$  for  $\theta_d$ , estimates for parameters of  $\theta$  can obviously be obtained, and in turn, feature  $B_1/A_1$  can be computed.

With the considered data, two different heterogeneous groups can be defined: "Grey/White", for a triplet of contacts with more grey matter between the first two contacts than between the last two ones, and "White/Grey", for the converse. In that case, 136 triplets are obtained with our data, and using scenarii with 75 % of the data for training, and the remaining 25 % for validation, classification results were obtained with an accuracy of  $73 \pm 6\%$  [21].

## IV. SINGLE CONTACT CLASSIFICATION RESULTS

Since in the former section, non-parametric and parametric identification methods were only considered for homogeneous and heterogeneous groups respectively (pre-selected according to MRI classification), and for contact pairs and triplets respectively, the purpose here is to discuss how they can be enhanced so as to end up with an *automatic classification* for *single contact*, and with *no prior knowledge*.

In our data, 356 triplets of contacts are now used, corresponding to those for which parametric models were validated in [21]. For each triplet, the non-parametric method is applied for the first two contacts, forming 356 pairs.

### A. Classification results with separate methods

Let us first discuss how previous identification approaches perform for the classification of a *single contact*, without any prior homogeneity or heterogeneity information. This means using pairs of contacts with non-parametric method, and triplets with parametric one as before, but now with the goal of identifying tissue for the first contact (of a triplet, or a corresponding pair). Classifying labels then reduce to "Grey", and "White", as in our gold standard MRI classification. Two LDA classifiers are trained, either considering non-parametric features (11)-(12) and only homogeneous pairs according to the MRI (145 "Grey/Grey", and 124 "White/White"), or

considering parametric feature ( $B_1/A_1$ , as emphasized in proposition 2) and only heterogeneous triplets according to the MRI (73 "Grey/White", and 63 "White/Grey").

Notice that a heterogeneous triplet can be related to a homogeneous pair, if the first two contacts of the triplet are in the same tissue, and the third one in a different tissue. For our pairs of contacts, 76% are in homogeneous tissue, and 24% in heterogeneous one. For the triplet, 56% are in homogeneous tissue, 38% in heterogeneous one, and 6% are in mixed tissue, where the intermediate contact is in a tissue different from the one of the other two contacts (tissue orders of the form Grey/White/Grey or White/Grey/White).

Classifier training (for first contacts) was done with 75 % of the data, and validated with the remaining 25 %. Trained classifiers were applied to pairs and triplets of contacts in homogeneous and heterogeneous groups first separately, and then to all 356 first contacts involved in the study. Accuracies of classification results obtained for each of those cases are summarized in Table I.

TABLE I: Accuracies of Identification-based LDA Classifiers for Single Contacts (for a set of 356 contacts)

LDA Classifier	Accuracy		
	Only homogeneous	Only heterogeneous	All contacts
Non-parametric	72% (76% of pairs)	55% (24% of pairs)	68%
Parametric	60% (56% of triplets)	73% (38% of triplets)	65%

As expected, the non-parametric classifier performs better for homogeneous groups, and the parametric classifier is better for heterogeneous ones. One can also notice that the parametric classifier gives a higher accuracy for homogeneous group separation than the non-parametric classifier for heterogeneous group separation. However, when looking at overall accuracy considering all groups, the non-parametric classifier outperforms the parametric one. This can be explained by the fact that 76% of contact pairs are in homogeneous tissues.

### B. Combination of Both Identification Methods

From the results of previous subsection, each identification-based classification method classifies well the label of the first contact for different types of tissue combinations. Here, the idea is to combine information provided by both classifiers, using the *posterior probabilities* of each first contact to be in the "Grey" group, according to each classifier, non-parametric ( $np$ ) or parametric ( $p$ ).

The classifier will be mentioned by an index  $c \in \{np, p\}$ , and features for a contact  $x$  in "Grey" group assumed to satisfy a Gaussian distribution density of the form:

$$P_c(x|G) = \frac{1}{((2\pi)^d |\Sigma_G|)^{\frac{1}{2}}} \exp\left(-\frac{1}{2}(x - \mu_G)\Sigma_G^{-1}(x - \mu_G)^T\right) \quad (22)$$

where  $d$  is the number of features ( $d = 4$  if  $c = np$ , and  $d = 1$  if  $c = p$ ), while  $\Sigma_G$  and  $\mu_G$  refer to covariance and mean of the features of group "Grey" respectively.

Denoting by  $P_G$  the prior probability of the "Grey" class (resp.  $P_W$  for "White" class) and defining a normalization coefficient by the following law of total probabil-

ity  $P(x) := \sum_{k \in \{G, W\}} P_c(x|k)P_k$ , the normalised posterior probability is obtained by Bayes rule as:

$$\hat{P}_c(G|x) = \frac{P_c(x|G)P_G}{P(x)} \quad (23)$$

The values of  $\hat{P}_c(G|x)$  indicate how likely the contact  $x$  is to be part of the "Grey" group, given its feature values. Each set of 356 pairs and 356 triplets is assigned a value of normalised posterior probability  $\hat{P}_{np}(G|x)$  and  $\hat{P}_p(G|x)$  corresponding to the non-parametric and parametric classifiers respectively.

This information can then be used to first identify contacts 'badly' classified, and then classify the remaining ones:

1) *Bad contacts elimination*: Contacts with a high probability of being badly classified can indeed be eliminated, by comparing labels provided by each classifier.

Over the 356 combinations of contacts, the elements obtaining same labels when using both non-parametric and parametric classifiers can be considered as correctly classified (72%). However, this does not mean that all of the remaining 28% should be considered as "badly" classified. In fact, for the cases where the obtained probability is around 0.5 (say  $0.4 < \hat{P}_c(G|x) < 0.6$ ) with either non-parametric or parametric classifier, the chances for the contact to be in grey or white matter are quite similar according to this classifier. Hence the idea in such cases is to rather refer to the other classifier to make a decision, and there is no error of classification. Thus, the only classifications that can be considered as "bad" when comparing labels obtained by the two classifiers are those for which when one of the normalised posterior probabilities is high the other one is low. With that, only 14% of contacts can be considered as "badly" classified, leaving 305 contacts to be analysed in the following step.

A summarizing picture of this bad classification identification based on normalised posterior probabilities is given in Figure 13, together with the likely triplet compositions expected for each combination of probabilities.

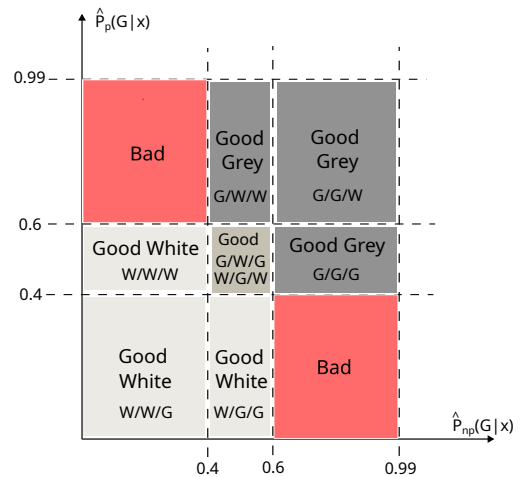


Fig. 13: Illustration of the "Bad" contact identification process based on normalised posterior probabilities.

2) *Combined classification*: After elimination of badly classified contacts, combination of information delivered by each classifier can be considered for remaining contacts. To that end, an average normalised posterior probability is defined from the normalised posterior probabilities of each classifier (equation (23)):

$$\hat{P}(G|x) = \frac{\hat{P}_{np}(G|x) + \hat{P}_p(G|x)}{2} \quad (24)$$

On this basis, we adopt the following classification:

- if  $\hat{P}(G|x) > 0.5$ , the contact is considered to be in "Grey" matter,
- if  $\hat{P}(G|x) < 0.5$  the contact is considered to be in "White" matter.

With this approach, applied to the 305 contacts previously selected, the obtained accuracy w.r.t. MRI classification is 72%.

In order to compare this combined classification with performances by each separate classifier, pairs and triplets in the same 305 selected contacts are used. The results are shown in Figure 14, presenting the percentage of correctly classified first contacts by combined classification in comparison to the percentage of correctly classified first contacts by each of the classifiers separately, in pairs and triplets for the non-parametric and parametric cases respectively.

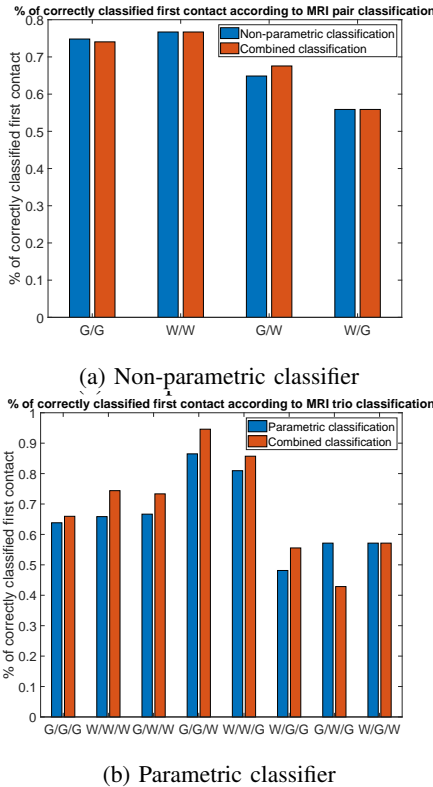


Fig. 14: Comparison of correctly classified first contacts with (a) non-parametric and combined classifiers, and (b) parametric and combined classifiers (G means Grey and W White).

Table II also displays the overall accuracies for each classifier with all 305 contacts.

TABLE II: Accuracies for Single Contact Classification for Each Classifier approach with 305 Contacts

	Accuracy
Combined	72%
Non-parametric	72%
Parametric	66%

From those results, it can be noticed that the combined classifier has a performance very similar to that of non-parametric classifier. With the elimination of "Bad" contacts, the performance of individual classifiers was enhanced when compared to Table I.

In the upper part of Figure 14, it can be seen that even if performances are pretty similar, the combined classification does a bit better than the non-parametric one for classification of "Grey/White" cases.

On the other hand, in the lower part, it appears that this combined classifier has a better performance than the parametric one for all cases, except configurations "Grey/White/Grey" and "White/Grey/White". The accuracy can even reach almost 95% for the "G/G/W" case, and Table II shows an average improvement from 66% for the parametric classifier by itself, to 72% with the combined one.

## V. CONCLUSIONS

In this paper, two transfer function modelling approaches for dynamic representation of brain-electrode interface in SEEG have been reviewed, with the purpose of using them for brain tissue classification (grey or white matter) around each electrode contact. A first one is based on pairs of contacts and frequency-based non-parametric identification, showing good classification results for contacts in homogeneous matter. On the other hand, the second approach is based on triplets of contacts and impedance-based parametric identification, providing good classification results for contacts in heterogeneous matter. On this basis, the extension of those separate methods to a combined framework allowing for tissue classification of single contacts and with no homogeneous or heterogeneous prior information has been presented, in the end giving classification results with accuracies larger than 70%. This is promising, and future studies will be dedicated to accuracy improvements and data-based tests enlargement.

## APPENDIX

Proof of proposition 1:

Considering the structure of circuit in Figure 7, with  $Z_b = R_{med}$  as in Figure 10, let us set  $Z_k := Z + R_{medk} + Z$  for  $k = 1, 2$ . Then it easily follows (voltage divider):

$$\mathcal{L}(V_2)(s) = \frac{Z_2}{Z_1 + Z_2} \mathcal{L}(V_1)(s) \quad (25)$$

On the other hand, with notations of Figures 8 and 9, the definition of  $Z$  yields:

$$Z = Z_i + Z_p \quad (26)$$

where

$$\begin{aligned} Z_i &= \frac{Z_{CPEDl}R_{ct}}{Z_{CPEDl} + R_{ct}} \\ &= \frac{R_{ct}}{1 + R_{ct}Q_{dl}s^\alpha} \end{aligned} \quad (27)$$

and

$$\begin{aligned} Z_p &= R_{en} + \frac{Z_{CPPEcl}R_{cl}}{Z_{CPPEcl} + R_{cl}} \\ &= R_{en} + \frac{R_{cl}}{1 + R_{cl}Q_{cl}s^\alpha} \end{aligned} \quad (28)$$

Hence  $Z = N/D$  with:

$$\begin{aligned} N &= R_{en}(1 + R_{cl}Q_{cl}s^\alpha)(1 + R_{ct}Q_{dl}s^\alpha) \\ &\quad + R_{cl}(1 + R_{ct}Q_{dl}s^\alpha) + R_{ct}(1 + R_{cl}Q_{cl}s^\alpha) \\ D &= (1 + R_{cl}Q_{cl}s^\alpha)(1 + R_{ct}Q_{dl}s^\alpha) \end{aligned} \quad (29)$$

Then:

$$\frac{Z_2}{Z_1 + Z_2} = \frac{2N + R_{med2}D}{4N + (R_{med1} + R_{med2})D} \quad (30)$$

By expanding denominator expression, we get its constant term as  $4(R_{ct} + R_{cl} + R_{en}) + R_{med1} + R_{med2}$ , and normalizing by it all coefficients in expanded numerator and denominator, coefficients  $B_i$ 's and  $A_i$ 's of proposition 1 are obtained.

#### REFERENCES

- [1] G. Besançon, G. Becq, and A. Voda. Fractional-order modeling and identification for a phantom eeg system. *IEEE Transactions on Control Systems Technology*, 28(1):130–138, 2020.
- [2] G. Besançon, A. Voda, G. Becq, and M. Machado. Order and parameter identification for a non-integer-order model of an eeg system. *IFAC-PapersOnLine (SISYD 2018)*, 51(15):772–777, 2018.
- [3] M. Brodie, S. Shorvon, R. Canger, P. Halasz, S. Johannessen, P. Thompson, H. Wieser, and P. Wolf. Commission on european affairs: appropriate standards of epilepsy care across europe. *Epilepsia*, 38(11):1245–1250, 1997.
- [4] A. Carvallo, J. Modolo, P. Benquet, S. Lagarde, F. Bartolomei, and F. Wendling. Biophysical modeling for brain tissue conductivity estimation using seeg electrodes. *IEEE Transactions on Biomedical Engineering*, 66(6):1695–1704, 2018.
- [5] O. David, A. Job, L. De Palma, D. Hoffmann, L. Minotti, and P. Kahane. Probabilistic functional tractography of the human cortex. *Neuroimage*, 80:307–317, 2013.
- [6] R. De Levie. The influence of surface roughness of solid electrodes on electrochemical measurements. *Electrochimica Acta*, 10(2):113–130, 1965.
- [7] P. Deman, M. Bhattacharjee, F. Tadel, A. Job, D. Rivière, Y. Cointepas, P. Kahane, and O. David. Intranat electrodes: a free database and visualization software for intracranial electroencephalographic data processed for case and group studies. *Frontiers in neuroinformatics*, 12:40, 2018.
- [8] A. Djouambi, A. Voda, and A. Charef. Recursive prediction error identification of fractional order models. *Communications in Nonlinear Science and Numerical Simulation*, 17(6):2517–2524, 2012.
- [9] L. Dora, S. Agrawal, R. Panda, and A. Abraham. State-of-the-art methods for brain tissue segmentation: A review. *IEEE reviews in biomedical engineering*, 10:235–249, 2017.
- [10] R. Fisher, W. Boas, W. Blume, C. Elger, P. Genton, P. Lee, and J. Engel Jr. Epileptic seizures and epilepsy: definitions proposed by the international league against epilepsy (ilae) and the international bureau for epilepsy (ibe). *Epilepsia*, 46(4):470–472, 2005.
- [11] P. Greene, A. Li, J. González-Martínez, and S. Sarma. Classification of stereo-eeg contacts in white matter vs. gray matter using recorded activity. *Frontiers in neurology*, page 1806, 2021.
- [12] W. Grill and J. Thomas Mortimer. Electrical properties of implant encapsulation tissue. *Annals of biomedical engineering*, 22(1):23–33, 1994.
- [13] C. Ionescu, A. Lopes, D. Copot, J.A.T. Machado, and J.H.T. Bates. The role of fractional calculus in modeling biological phenomena: A review. *Commun Nonlinear Sci Numer Simulat*, 51:141–159, 2017.
- [14] S. Lempka, M. Johnson, M. Moffitt, K. Otto, D. Kipke, and C. McIntyre. Theoretical analysis of intracortical microelectrode recordings. *Journal of neural engineering*, 8(4):045006, 2011.
- [15] S. Lempka, S. Miocinovic, M. Johnson, J. Vitek, and C. McIntyre. In vivo impedance spectroscopy of deep brain stimulation electrodes. *Journal of neural engineering*, 6(4):046001, 2009.
- [16] S. Liang, R. Wu, and L. Chen. Laplace transform of fractional order differential equations. *Electron. J. Differ. Equ*, 139:2015, 2015.
- [17] L. Ljung. *System Identification: Theory for the User*. Pearson Education, 1998.
- [18] M. Machado, A. Voda, G. Besançon, G. Becq, P. Kahane, and O. David. Brain tissue classification from stereoelectroencephalographic recordings. *Journal of Neuroscience Methods*, 365:109375, 2022.
- [19] M. M. P. Machado, A. Voda, G. Besançon, G. Becq, O. David, and P. Kahane. Dynamic modelling of the brain-electrode interface for stereoelectroencephalography. In *International Conference on System Theory, Control and Computing, Sinaia, Romania*, 2022.
- [20] M. M. P. Machado, A. Voda, G. Besançon, G. Becq, O. David, and P. Kahane. System identification-based automatic brain tissue classification for stereoelectroencephalography. In *International Conference on System Theory, Control and Computing, Sinaia, Romania*, 2022.
- [21] M. M. P. Machado, A. Voda, G. Besançon, G. Becq, O. David, and P. Kahane. Electrode-brain interface fractional order modelling for brain tissue classification in SEEG. *Biomedical Signal Processing and Control*, 79:104050, 2023.
- [22] R. Magin and M. Ovadia. Modeling the cardiac tissue electrode interface using fractional calculus. *Journal of Vibration and Control*, 14(9-10):1431–1442, 2008.
- [23] E. McAdams and J. Jossinet. Tissue impedance: a historical overview. *Physiological measurement*, 16(3A):A1, 1995.
- [24] H. McCann, G. Pisano, and L. Beltrachini. Variation in reported human head tissue electrical conductivity values. *Brain topography*, 32(5):825–858, 2019.
- [25] U.R. Mohan, A.J. Watrous, J.F. Miller, B.C. Lega, M.R. Sperling, G.A. Worrell, R.E. Gross, K.A. Zaghloul, B.C. Jobst, K.A. Davis, S.A. Sheth, J.M. Stein, S.R. Das, R. Gorniak, P.A. Wanda, D.S. Rizzuto, M.J. Kahana, and J. Jacobs. The effects of direct brain stimulation in humans depend on frequency, amplitude, and white-matter proximity. *Brain stimulation*, 13(5):1183–1195, 2020.
- [26] K. Otto, M. Johnson, and D. Kipke. Voltage pulses change neural interface properties and improve unit recordings with chronically implanted microelectrodes. *IEEE transactions on biomedical engineering*, 53(2):333–340, 2006.
- [27] A. Oustaloup. *Diversity and non-integer differentiation for system dynamics*. Wiley, 2014.
- [28] I. Podlubny. *Fractional differential equations*. Elsevier Science, 1999.
- [29] D. Robinson. The electrical properties of metal microelectrodes. *Proceedings of the IEEE*, 56(6):1065–1071, 1968.
- [30] V. Sankar, E. Patrick, R. Dieme, J. Sanchez, A. Prasad, and T. Nishida. Electrode impedance analysis of chronic tungsten microwire neural implants: understanding abiotic vs. biotic contributions. *Frontiers in neuroengineering*, 7:13, 2014.
- [31] L. Trebaul, P. Deman, V. Tuyisenge, M. Jedynak, E. Hugues, D. Rudrauf, M. Bhattacharjee, F. Tadel, B. Chanteloup-Foret, C. Saubat, et al. Probabilistic functional tractography of the human cortex revisited. *NeuroImage*, 181:414–429, 2018.
- [32] S. Victor, P. Melchior, M. Pellet, and A. Oustaloup. Lung thermal transfer system identification with fractional models. *IEEE Transactions on Control Systems Technology*, 28(1):1–11, 2018.
- [33] A. Voda, A. Charef, D. Idiou, and M. Mulinari Pinheiro Machado. Creep modeling for piezoelectric actuators using fractional order system of commensurate order. In *21st International Conference on System Theory, Control and Computing (ICSTCC)*, 2017.